Journal of Membrane Science 502 (2016) 141–150

Contents lists available at ScienceDirect

Journal of Membrane Science

journal homepage: www.elsevier.com/locate/memsci

Dissolved methane recovery from anaerobic effluents using hollow fibre membrane contactors

J. Cookney, A. Mcleod, V. Mathioudakis, P. Ncube, A. Soares, B. Jefferson, E.J. McAdam *

Cranfield Water Science Institute, Cranfield University, Building 39, MK43 0AL, UK

ARTICLE INFO

Article history:
Received 13 May 2015
Received in revised form
15 December 2015
Accepted 19 December 2015
Available online 23 December 2015

Keywords:
Stripping
Degassing
Desorption
Fracking
Fugitive emission
Greenhouse gas

ABSTRACT

Hollow fibre membrane contactor (HFMC) systems have been studied for the desorption of dissolved methane from both analogue and real anaerobic effluents to ascertain process boundary conditions for separation. When using analogue effluents to establish baseline conditions, up to 98.9% methane removal was demonstrated. Elevated organic concentrations have been previously shown to promote micropore wetting. Consequently, for anaerobic effluent from an upflow anaerobic sludge blanket reactor, which was characterised by a high organic concentration, a nonporous HFMC was selected. Interestingly, mass transfer data from real effluent exceeded that produced with the analogue effluent and was ostensibly due to methane supersaturation of the anaerobic effluent which increased the concentration gradient yielding enhanced mass transfer. However, at high liquid velocities a palpable decline in removal efficiency was noted for the nonporous HFMC which was ascribed to the low permeability of the nonporous polymer provoking membrane controlled mass transfer. For anaerobic effluent from an anaerobic membrane bioreactor (MBR), a microporous HFMC was used as the permeate comprised only a low organic solute concentration. Mass transfer data compared similarly to that of an analogue which suggests that the low organic concentration in anaerobic MBR permeate does not promote pore wetting in microporous HFMC. Importantly, scale-up modelling of the mass transfer data evidenced that whilst dissolved methane is in dilute form, the revenue generated from the recovered methane is sufficient to offset operational and investment costs of a single stage recovery process, however, the economic return is diminished if discharge is to a closed conduit as this requires a multi-stage array to achieve the required dissolved methane consent of 0.14 mg l^{-1}.

1. Introduction

In engineered anaerobic environments such as landfills or anaerobic wastewater treatment processes, the process effluent produced is generally at equilibrium with the gas phase, a significant fraction of which is methane (CH_4, 50% to 80% v/v in gas phase) [1]. Consequently, anaerobic effluents commonly comprise between 10 and 25 mg l^{-1} of dissolved methane dependent upon the partial pressure of methane in the process atmosphere [2,3]. Several authors have also reported on anaerobic effluents that are 'supersaturated' with dissolved methane, which demonstrates that dissolved methane concentrations can be higher than those predicted based on Henry's law, ostensibly due to the formation of microbubbles [4,5]. Hartley and Lant [5] recorded an average supersaturation index of 1.6 (C_e/C^*, measured concentration in water/expected equilibrium concentration) from an ambient temperature high rate anaerobic migrating bed reactor treating crude domestic wastewater. The authors latterly estimated supersaturation indices of between 1.9 and 6.9 for previously published studies. Cookney et al. [3] also recorded an effluent supersaturation index of 1.6 when operating an upflow anaerobic sludge blanket reactor (UASB) for domestic wastewater treatment and importantly noted that dissolved methane accounted for over 50% of the methane produced, which constrains the opportunity for energy generation from full flow anaerobic treatment and will inevitably broaden carbon footprint [6].

Dissolved methane must be removed from anaerobic effluents that are to be discharged to sewer or other enclosed conduits to avoid generating potentially explosive atmospheres. The lower explosive limit (LEL) for methane in the gas phase is 5% v/v which at equilibrium corresponds to a dissolved methane concentration of 1.4 mg l^{-1} at 15 °C and 101.325 kPa [7]. Consequently, a factor of safety of ten has been applied in industry to ensure that explosive conditions are avoided, leading to a dissolved methane discharge consent of 0.14 mgCH_4 l^{-1} often being enforced [2]. Multi-stage

* Corresponding author.
E-mail address: e.mcadam@cranfield.ac.uk (E.J. McAdam).

http://dx.doi.org/10.1016/j.memsci.2015.12.037
0376-7388/

bubble column cross-flow cascades or forced draft aerators are generally used to provide contact between the methane saturated liquid phase and a dilute gas phase (air or nitrogen) which introduces a concentration gradient at the gas–liquid interface to create the driving force for stripping. Both processes yield a compliant effluent, however, considerable process scale is demanded to enable sufficient contact time [8]. Furthermore, significant air flows are required which produce a dilute gas phase below the LEL for methane (around 0.03%CH_4 v/v in the stripped gas) [2,8].

Micro-porous hollow-fibre membrane contactors enable the same desorption mechanism to conventional bubble columns through mediating contact between the gas and liquid phases. However, the hydrophobic micro-porous membrane supports non-dispersive contact between the liquid and gas phases where the dissolved gas is free to diffuse through the gas filled pores [9]. Furthermore, the hollow-fibre geometry yields higher packing densities leading to large specific surface areas which enable reduced process scale and lower gas-to-liquid ratios to be employed. For example, O'Haver et al. [10] demonstrated superior removal efficiencies with a HFMC compared to an aerated bubble column for desorption of volatile organic compounds (VOCs) from a contaminated surface stream requiring a unit volume only 7.5% of the column [10]. Hydrophobic micro-porous HFMC have also seen wide commercial deployment for oxygen (O_2) desorption from high quality industrial process waters [11]. However, their application to wastewater is more limited since wastewater comprised of concentrated organic solutes have been shown to induce membrane wetting of the micro-pores, a process whereby water penetrates the gas filled pore (either partially or fully) impeding gas transport [12,13].

To obviate the wetting phenomenon, nonporous membranes have instead been used as the boundary between the liquid and gas phase [9]. Both Bandara et al. [14] and Cookney et al. [3] have employed nonporous membranes (composite with polyethylene as the nonporous substrate [14]; symmetric polydimethylsiloxane, PDMS [3]) for dissolved methane recovery from the anaerobic effluent of UASB reactors which are noted to comprise both particulate and soluble organics. In their study, Bandara et al. [14] were able to successfully demonstrate that the methane recovered was of a viable concentration for reuse in energy generation. However, the authors did not seek to optimise the hydrodynamic environment and as such residence times within the membrane vessel were between 2.8 and 9.2 h which are practically unsustainable at full scale. Cookney et al. [3] undertook preliminary investigation of the hydrodynamic environment and determined that maximum dissolved methane removal efficiency (72%) was achieved at the lowest liquid velocity trialled but the authors did not explicitly investigate rate limiting phenomena thus the boundary conditions for methane recovery were not clearly identified. Both nonporous HFMC studies applied wastewater to the shell-side of the membrane to avoid the risk of clogging the fibre lumen with particulate matter. It is encouraging that the adoption of wide bore fibres by Cookney et al. [3] generated sufficient interstitial spacing (packing fraction of 0.43) to avoid the onset of fouling or clogging of the surrounding channel.

However, in nonporous membranes, it has been established that the membrane wall can present a significant resistance to mass transfer as the gases have to diffuse through the dynamic free volume network of the polymer [9]. Thus whilst both nonporous HFMC studies importantly identified the potential for dissolved methane recovery from UASB effluents, micro-porous hollow-fibre membranes would be preferentially selected for dissolved methane removal where anaerobic effluents are sufficiently low in organic solutes to limit wetting phenomena as this will enhance mass transfer and limit process scale. Several authors have now proposed the use of anaerobic membrane bioreactors (AnMBR) as an alternative reactor configuration to UASB reactors since the micro or ultrafiltration membrane that is integrated into the process can produce permeate that is free of particulate matter (suspended solids) and is low in organic solutes [15]. As a consequence of the low organic solute concentration, microporous HFMC could be considered appropriate for application to AnMBR permeate for dissolved methane recovery. Furthermore, the anaerobic permeate can be applied to the lumen-side of the microporous membrane due to the absence of particles, which has been noted to provide preferential mass transport in microporous HFMC at pilot scale [19].

From a review of the literature, very different attributes (membrane material and fibre packing density) are required when applying hollow fibre membrane contactor technology to the two principle anaerobic reactor configurations (AnMBR or UASB) considered for anaerobic wastewater treatment. Specifically, for effluent comprised of high organics and high solids concentration (typical of UASB reactors), hollow-fibres comprised of nonporous material are advantageous as they limit wetting phenomena; loose fibre packing is also advantageous as this limits clogging of the interstitial fibre spacing [3]. In contrast, the high permeate quality produced from an AnMBR (no solids, low organics) suggests HFMC comprised of microporous material and higher packing density can be used, which would advantage mass transfer, as the risks of wetting and clogging are obviated. The aim of this study is therefore not to provide a direct comparison of porous and nonporous HFMC for dissolved methane recovery but is instead to examine application of HFMC technology to the recovery of dissolved methane from the two principle anaerobic reactor configurations considered for full scale wastewater treatment. Specific objectives are to: (i) to establish baseline mass transfer data for two selected HFMC designs within a controlled environment using an analogue effluent; (ii) examine dissolved methane recovery from UASB reactor effluent using nonporous HFMC, with liquid flow on the shell-side, to avoid the risk of wetting and lumen blockage by particulate and soluble organics; (iii) examine dissolved methane recovery from AnMBR reactor permeate using microporous HFMC, with liquid flow on the lumen-side to maximise mass transfer in anaerobic permeate comprised of no particulates and only a low organic solute concentration; and (iv) use baseline mass transfer data generated from analogue effluents to benchmark and diagnose HFMC performance on real effluent.

2. Materials and methods

2.1. Experimental set-up

The PDMS HF membrane contactor comprised 13 dense polydimethylsiloxane fibres with a 250 μm wall and 3.2 mm lumen diameter (Sterilin Limited, Newport, UK) (Table 1). The fibre ends were pre-treated with sealant to enhance adhesion (Dow Corning, Seneffe, Belgium) and potted into a PVC shell (23 mm internal diameter) using a mixture of epoxy resin/polyolefin primer (FredAldous, Manchester, UK; Loctite, Henkel, Germany). The PDMS membrane yielded a 0.62 m fibre length with total contact area 0.094 m^2 and packing fraction (ø) 0.34. The packing fraction and fibre outer diameter were specified similar to a previous HFMC study which evidenced limited fouling/clogging in HFMC applied to real wastewater comprising particulate matter [3]. The PDMS membrane was operated counter-currently with water flowing parallel to the fibres on the shell-side to avoid the risk of lumen clogging. Nitrogen enriched air was produced from compressed air (8 barg) using a nitrogen selective HF membrane (5-M, N_2 Gen. Ltd., London, UK) and introduced into the HF lumen. Nitrogen gas

Table 1
Membrane module characteristics.

Parameter		PDMS (Nonporous)	PP (Microporous)
Membrane Surface			
Pore size	(μm)	N/a	0.03/ < 0.1[a]
Porosity	(%)	N/a	40
Fibre description			
Inner diameter	(μm)	3200	220
Outer diameter	(μm)	3700	300
Wall thickness	(μm)	250	40
Fibre length	(m)	0.62	0.1397
Module design			
Shellside diameter	(m)	0.023	0.0425
Shellside volume	(ml)	257	78
No. of fibres	(dimensionless)	13	7400
Total fibre area	(m^2)	0.094	0.58[b]
Packing	($m^2\ m^{-3}$)	364	4600

[a] Fibre diameter longer along fibre length.
[b] Based on fibre inner diameter.

flow rate was controlled using a needle valve (0–25 l min^{-1}, Key Instruments, Trevose, US). The microporous membrane contactor comprised 7400 fibres (ø 0.37) creating a surface area of 0.58 m^2. The fibre contained a 40 μm wall and 220 μm lumen diameter (Membrana, Wuppertal, Germany). The pores of the microporous polypropylene fibres were around 30 nm in width and 100 nm in length [9]. Water was passed through the lumen of the microporous HFMC to maximise mass transfer (which aligned with manufacturer recommendations [19] and was considered appropriate as the AnMBR permeate was particle free) whilst nitrogen gas was introduced in counter-current mode to the shell-side (Fig. 1). The water line was fitted upstream and downstream of the membrane with gas tight sampling ports comprised of stainless steel luer-lock fittings to enable liquid samples to be collected without exposure to the atmosphere.

2.2. Analytical methods

The method for dissolved methane analysis was adapted from Alberto et al. [16]. Gas chromatograph vials (22.7 ml) were sealed with butyl lined caps and placed under vacuum (280 mbar, Capex L2C vacuum pump, Charles Austen Pumps, Byfleet, UK). Evacuated vials were then fixed onto the water line via the luer-lock fittings to enable closed atmosphere sampling. Samples were collected until pressure equilibrated leaving a headspace of *ca.* 5 ml. An accurate determination of the liquid volume collected was determined by measuring vial weight before and after liquid collection using a three decimal place balance. Following collection, samples were agitated for 7 min and left for 16 h to enable equilibration with the headspace [3]. Prior to sample collection, three liquid-side retention times were completed to ensure that steady-state was reached; samples were collected in triplicate for each set of conditions. Analysis of the headspace gas phase was carried out using gas chromatograph with thermal conductivity detection (GC-TCD, 200 Series, Cambridge Scientific Instruments, Cambridge, UK). With each analysis, reference gas mixtures (methane 5, 24.97, 49.97 and 74.99% balanced with N_2) were used to develop a calibration curve (Scientific Technical Gases Limited, Newcastle-Under-Lyme, UK). The final dissolved gas concentration was calculated using the following mass balance [5]:

$$X_{L1} = \frac{X_{G2}(Vol_G + \alpha Vol_L) - X_{G1}Vol_G}{Vol_L} \quad (1)$$

where X_{L1}, X_{G1} and X_{G2} are the dissolved gas concentration, gas headspace concentration before shaking and after shaking respectively (mg ml^{-1}), Vol_L and Vol_G are the liquid gas phase volumes in the vial (ml) and α is the Bunsen solubility coefficient. All dissolved methane measurements were performed in triplicate.

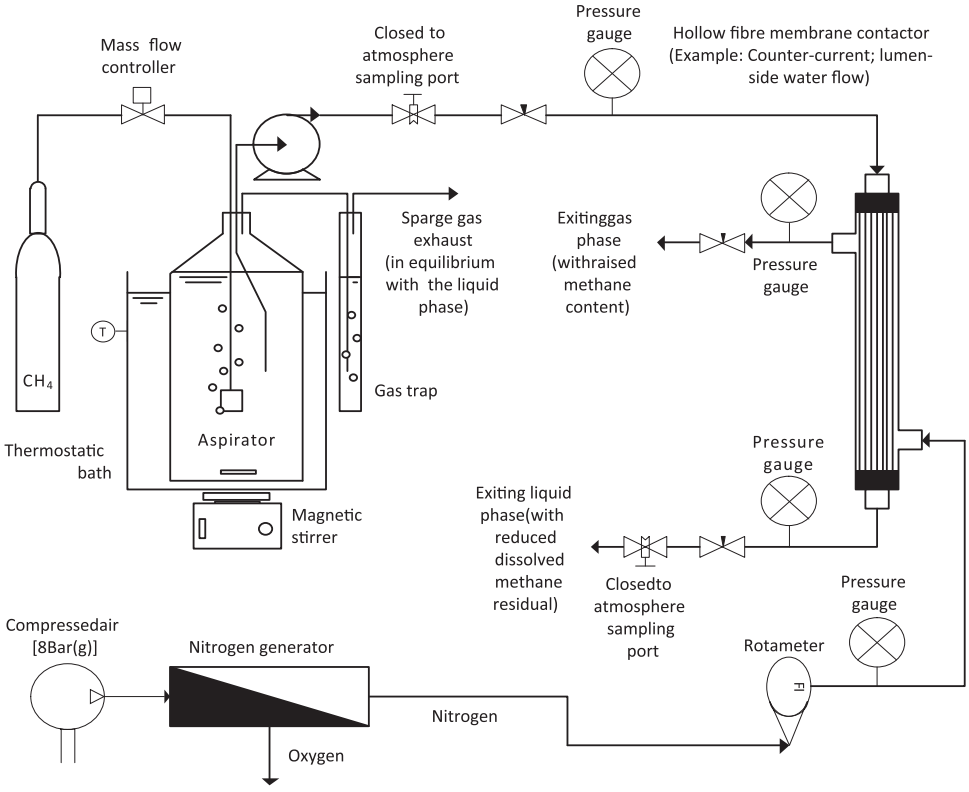

Fig. 1. Experimental rig schematic illustrating aspirator set-up for controlled production of synthetic wastewater.

2.3. Effluent production

Synthetic methane saturated effluents were prepared by sparging de-ionised (DI) water ($<1\ \mu S\ cm^{-1}$, Elga Process Water, Marlow, UK) with 99.995 % methane (BOC, Manchester, UK) using a 0.01–1 l min^{-1} mass flow controller (Alicat Scientific, Tucson, US) to control sparge rate. A magnetic stirrer was added to the sealed 22 l aspirator to enhance the rate at which saturation (equilibrium) was achieved (around 60 min). The aspirator was maintained at 25 °C and exposed to methane rich gas-side conditions (methane mole fraction of gas phase (y_{CH_4}) was 100%) yielding an average dissolved methane concentration at equilibrium of around 21 $mgCH_4\ l^{-1}$ in the analogue which is close to the equilibrium concentration estimated using a Bunsen solubility coefficient of 0.03469 (ml CH_4 (STP) [ml H_2O]$^{-1}$) [30]. The standard deviation of each triplicated inlet reading was below 3%. Throughout testing with the synthetic effluent, the average inlet dissolved methane concentration varied by less than 4.3% ($n=21$). Gas collected in the 2 l headspace was vented through a gas trap to release pressure and prevent supersaturation of the synthetic solution. Real methane saturated anaerobic effluents were also produced from an UASB and an anaerobic MBR. When testing anaerobic effluent, the aspirator was replaced with a 10 l capacity buffer tank which was directly filled from the UASB or AnMBR effluent line. The 42.5 l UASB comprised a granular biomass treating settled sewage at ambient temperature (mean temperature 18 °C, COD_T influent 360 mg l^{-1}) and was operated at a hydraulic retention time of 9.4 h, yielding an organic loading rate of 0.9 g l^{-1} d^{-1}. The anaerobic MBR comprised the 42.5 l UASB linked to a polyvinyldifluoride (PVDF) ultrafiltration hollow-fibre membrane downstream (nominal pore size, 0.04 μm; surface area 0.93 m^2). In both configurations, a recirculating flow was provided by recycling UASB effluent (for the AnMBR indirectly through the membrane chamber) to provide an internal upflow velocity of around 1 m h^{-1}.

2.4. Mass transfer analysis

If the influent gas phase concentration is assumed equal to zero, and the influent liquid-phase concentration is in equilibrium with the exiting air, the dimensionless Henry's constant (H for methane, 28.41 at 25 °C) can be used to estimate the minimum gas-to-liquid ratio necessary to achieve a set treatment objective [29]:

$$\left(\frac{Q_G}{Q_L}\right)_{min} = \frac{C_0 - C_e}{HC_0} \tag{2}$$

where Q_G is gas flow rate ($m^3\ h^{-1}$), Q_L is liquid flow rate ($m^3\ h^{-1}$) and c_0 and c_e are the inlet and outlet concentrations respectively. The overall mass transfer coefficient can be determined by a mass balance of dissolved methane in the water passing in the module [20]:

$$0 = -Q\frac{dc}{dA} - k\left(c_e - c^*\right) \tag{3}$$

where A is the total membrane area, and c_e and c^* are the actual and equilibrium concentrations of dissolved methane in the water. In this study, the nitrogen sweep gas is applied in excess, so the concentration c^* can be regarded as constant thus Eq. (3) can be integrated assuming that the inlet concentration is C_0 and can be conveniently expressed as [20]:

$$K_L = -\frac{V_L}{aL}\ln\left(\frac{c_e - c^*}{c_0 - c^*}\right) \tag{4}$$

where V_L is the superficial liquid velocity (m s^{-1}), a is the area per membrane volume of the bed (m^{-1}) and L is the membrane length in the direction of flow (m). Individual contributions to overall resistance for a hydrophobic microporous membrane with gas filled pores can be estimated:

$$\frac{1}{K_L} = \frac{H}{k_g} + \frac{H}{k_m} + \frac{1}{k_l} \tag{5}$$

where k_g, k_m and k_l are the gas, membrane and liquid coefficients respectively. The specific contribution to mass transfer provided by the micro-porous membrane (k_m) can be estimated by assuming unrestricted gas flow (i.e. not Knudsen diffusion) in a gas filled pore [18]:

$$k_m = \frac{D_g \varepsilon_m}{\tau_m l_m} \tag{6}$$

where ε_m, τ_m, and l_m are the porosity (40%), tortuosity (2.25) and thickness of the membrane respectively and D_g is the effective diffusion coefficient of gas filled pores [9]. In the absence of a limiting gas phase, and for sparingly soluble gases, this reduces to $1/K_L = 1/k_l$ indicating liquid film controlled mass transfer. For dense membrane contactors applied to desorption, the overall resistance to mass transfer is [17]:

$$\frac{1}{K_L} = \frac{\delta}{PH} + \frac{1}{k_l} \tag{7}$$

where δ/PH is the membrane resistance, δ is polymer thickness and P is polymer permeability.

3. Results

3.1. Impact of gas and liquid velocity on dissolved methane removal efficiency

For both membrane systems, high dissolved methane removal efficiencies (defined by the difference between the inlet and outlet dissolved methane concentrations entering and exiting the membrane) of 92.6% and 98.9% were recorded for the nonporous and micro-porous membrane systems respectively at the lowest liquid velocity (V_L) tested (4×10^{-4} m s^{-1} respectively). However, for both membrane systems dissolved methane removal efficiency decreased with an increase in V_L (Fig. 2). This trend was particularly pronounced for the nonporous PDMS membrane. To illustrate, removal efficiency declined rapidly from 92.6% to 40.8%

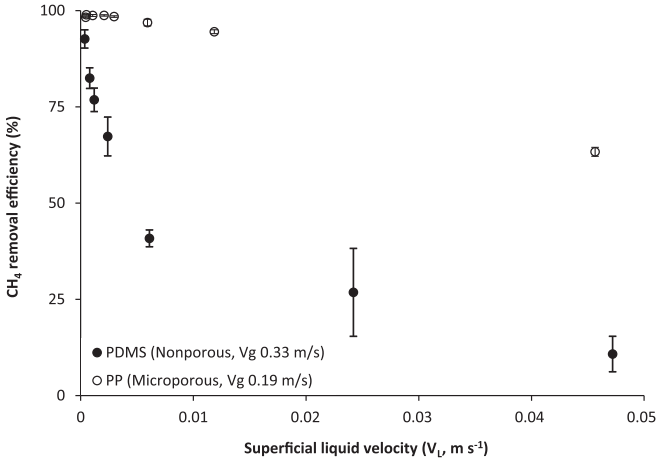

Fig. 2. Impact of superficial liquid velocity (V_L) on dissolved methane removal efficiency for the dense (PDMS) and microporous (polypropylene) membrane contactors. Gas velocity (V_G) fixed at 0.33 and 0.19 m s^{-1} for the nonporous and microporous membranes respectively.

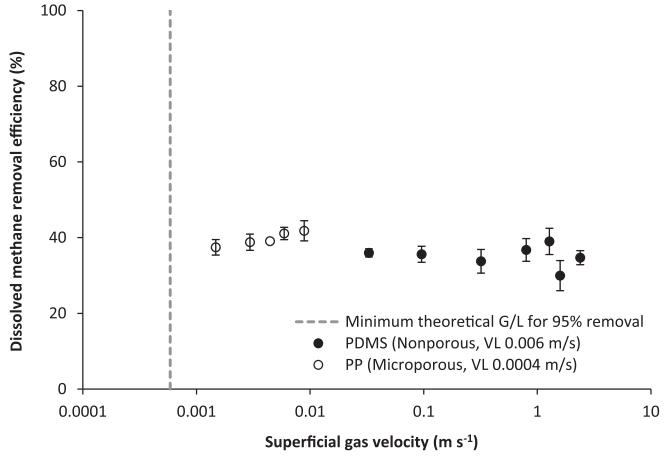

Fig. 3. Impact of superficial gas velocity (V_g) on dissolved methane removal efficiency for the dense (PDMS) and microporous (polypropylene) membrane contactors. Liquid velocity (V_L) fixed at 0.006 and 0.0004 m s^{-1} for the nonporous and microporous membranes respectively. Dashed line represents V_g necessary to achieve G/L_{min} for 95% removal.

when V_L was increased from 4×10^{-4} to 6×10^{-3} m s^{-1} and more gradually upon increasing V_L to 0.047 m s^{-1} where a dissolved methane removal efficiency of 10.8% was recorded. For comparison, dissolved methane removal efficiency decreased to 63.3% in the micro-porous membrane system when V_L was increased to 0.045 m s^{-1}. The influence of gas side hydrodynamics was also evaluated at fixed V_L (Fig. 3). For both membrane systems, dissolved methane removal efficiency remained relatively unchanged upon increasing V_G from 1.5×10^{-3} to 9×10^{-3} m s^{-1} and from 0.033 to 2.39 m s^{-1} for the micro-porous and nonporous membranes respectively.

3.2. Mass transfer analysis of microporous and dense membranes using synthetic effluent

Whilst dissolved methane removal efficiency was observed to decline with an increase in V_L, an increase in V_L was simultaneously noted to increase mass transfer (K_L) for both membrane systems (Figs. 4 and 5). The subsequent relationship observed between K_L and V_L for the nonporous membrane when treating synthetic effluent was ostensibly similar to that described

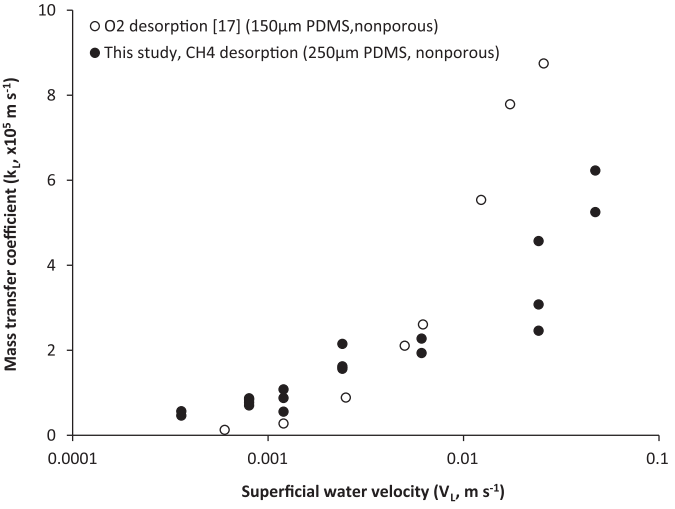

Fig. 4. Impact of superficial liquid velocity (V_L) on the overall mass transfer coefficient for the nonporous membrane contactor (PDMS, 250 μm wall thickness). Data compared to O_2 desorption data [17] from a PDMS (150 μm wall thickness) membrane.

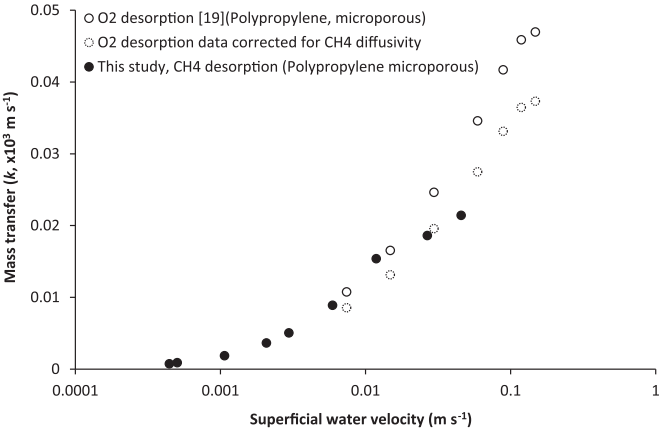

Fig. 5. Impact of superficial liquid velocity (V_L) on the overall mass transfer coefficient for the microporous membrane contactor. Dissolved oxygen data from the literature [19] which uses the same membrane has been added with and without correction of the mass transfer coefficient for the diffusivity of methane.

Bessarabov et al. [17] for the separation of dissolved oxygen from pure water using a flat sheet PDMS membrane (Fig. 4). Similarly for the micro-porous membrane, the data provided a reasonable fit to literature data for dissolved oxygen removal from pure water using the same fibre type [19] (Fig. 5). Experimental data was characterised in the dimensionless form of the Sherwood number ($Sh = Kd/D$) and provided a positive increase in Sh with an increase in V_L (Fig. 6). Tan et al. [21] provide a corrected Sherwood correlation of $Sh = 3.228Re^{0.5632}Sc^{0.33}$ for a PDMS hollow fibre membrane operated in shellside flow for removal of dissolved oxygen into a nitrogen sweep gas which substantially overpredicts mass transfer within this study. The relationship between Sh and Re in shell-side flow is strongly dependent upon both configuration and fibre packing [21]. However, broad agreement was identified between Sh data from the nonporous membrane system in this study and the general correlation proposed by Wickramasinghe et al. [20] following dissolved oxygen desorption trials of a host of membrane contactor architectures operated with water flowing on the shellside of $Sh = 0.8Re^{0.47}Sc^{0.33}$. Since the micro-porous HFMC was operated in lumen-side flow (in accordance with manufacturers instruction), the data produced could be adequately described by analogy to the Lévèque solution ($Sh = 1.62(Gz)^{1/3}$, valid for $Gz > 20$) once V_L exceeded 6×10^{-3} m s^{-1} which corresponded to a Gz range between 7 and 51. The difference in magnitude between Sherwood numbers produced from each membrane can be

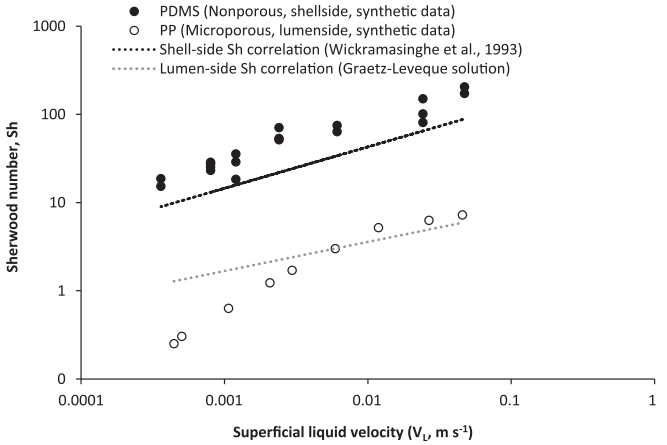

Fig. 6. Sherwood correlation for the dense (PDMS) and microporous (polypropylene) membrane contactors compared to established Sh correlations for lumen-side (Graetz-Lévêque solution, microporous) and shell-side flow [20].

accounted for by differences in equivalent diameter which is much smaller for lumen side flow (applied for the micro-porous membrane) than for shell side flow (applied for the PDMS membrane) even though the mass transfer coefficients are similar [21].

3.3. Mass transfer analysis of microporous and nonporous membranes using real effluent

Dissolved methane in the anaerobic effluent of the anaerobic membrane bioreactor measured 8.8 mg l^{-1} which approximately corresponds to the equilibrium concentration estimated for the methane mole fraction of the biogas produced within the headspace (y_{CH_4}0.41) indicating that the process effluent dissolved methane concentration was at saturation (C_e/C^* 1). The dissolved methane concentration in the UASB effluent was considerably higher at 25.4 mg l^{-1}, and exceeded the equilibrium concentration estimated for the methane mole fraction of the biogas produced within the headspace (0.76) which indicates supersaturation of the fluid (C_e/C^* 1.3), as has been demonstrated previously for anaerobic effluents [3,5]. Mass balance of the methane inventory demonstrates that for the systems studied, between 45% and 88% of the methane produced is released in dissolved form in the liquid phase. Experimental data was characterised through analysis of the Sherwood number across a range of V_L and was compared to that of the analogue (Figs. 8 and 9). Good parity was observed between *Sh* data derived from the synthetic and anaerobic MBR effluents with the microporous membrane. However, when comparing *Sh* data produced from analysis of the UASB effluent and analogue effluent, the UASB effluent *Sh* data was generally considerably higher than expected.

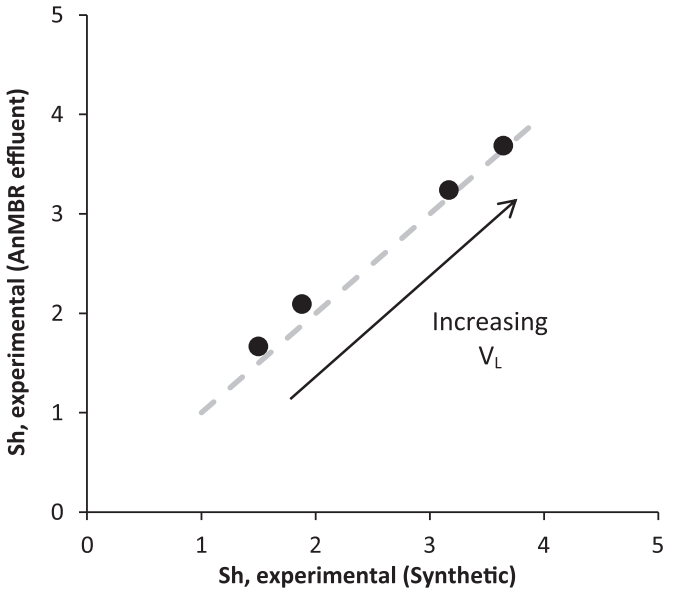

Fig. 8. Comparison of the Sherwood number (*Sh*) derived experimentally using synthetic effluent in the microporous contactor to the *Sh* number determined experimentally when using real effluent from an AnMBR. Dashed line represents a 1:1 relationship.

4. Discussion

4.1. Evaluation of process boundary conditions

In this study, the boundary conditions necessary to provide dissolved CH_4 removal efficiencies exceeding 98% in a single module have been demonstrated and require low applied superficial liquid velocities of around 0.003 m s^{-1}. When analysing process boundary conditions, the gas phase was noted to provide limited resistance to mass transfer which was evidenced by a negligible change in dissolved CH_4 removal efficiency having decreased V_G by over an order of magnitude (Fig. 2). This is analogous to behaviour reported by Tan et al. [21] during their study of dissolved oxygen (O_2) removal using a PDMS hollow fibre membrane, where removal efficiency remained stable following a decrease in gas flow from *G*/*L* 24:1 to 4:1. The non-limiting behaviour of the gas phase can be ascribed to the high volatility of methane which is characterised by a high Henry's constant ($H_{dimensionless}$ 28.41). Through application of the Henry's constant, a minimum *G*/L_{min} 0.034 is theoretically required to achieve 98% removal efficiency (Fig. 3). Consequently, provided the operational *G*/*L* exceeds *G*/L_{min}, gas phase resistance can be neglected and the overall resistance to mass transfer ($1/K_L$) simplifies to the sum of liquid ($1/k_L$) and membrane resistances ($1/k_m$). Importantly, low

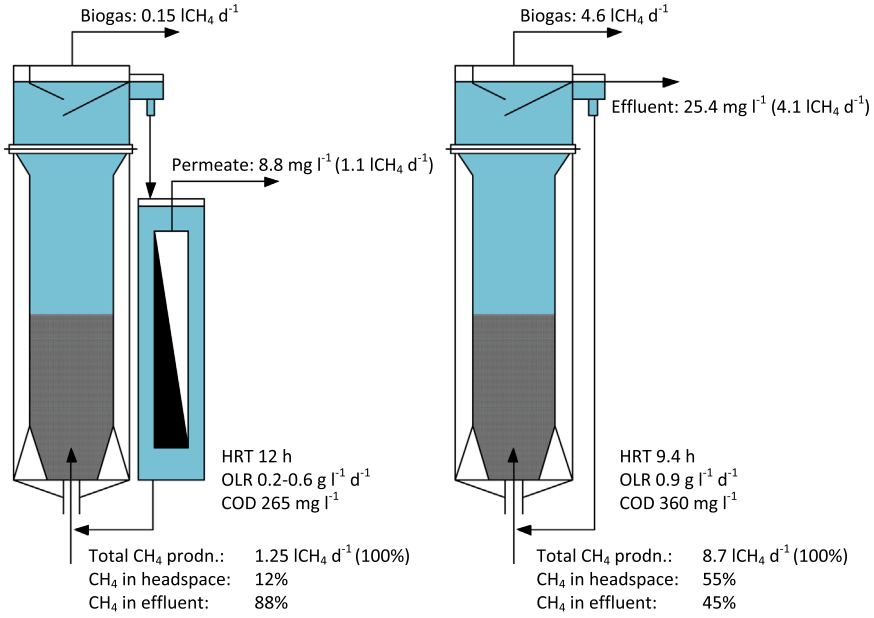

Fig. 7. Dissolved methane mass balance of the upflow anaerobic sludge blanket (UASB) reactor and anaerobic membrane bioreactor (AnMBR) configurations studied.

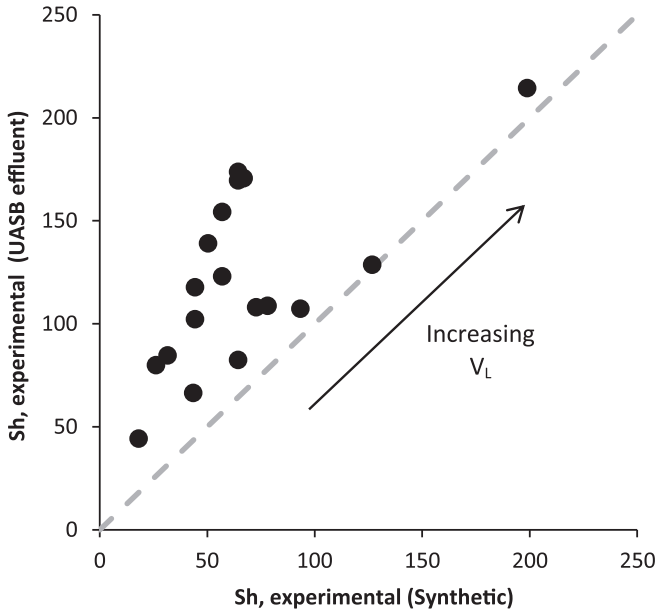

Fig. 9. Comparison of the Sherwood number (*Sh*) derived experimentally using synthetic effluent in the nonporous (PDMS) contactor to the *Sh* number determined experimentally when using real effluent from an AnMBR. Dashed line represents a 1:1 relationship.

sweep gas flows will also enable higher CH_4 content in the recovered gas phase. For example, a simplified mass balance at a *G*/*L* ratio of 0.034 suggests a final sweep gas comprising 53% methane which is sufficient for use in electricity production [22]. Bandara et al. [14] provided preliminary evidence to this effect when using partial pressure to control migration of dissolved methane through a polyethylene composite membrane. The authors recorded around 20% CH_4 in the gas phase and in fact regarded this to be an underestimation of the methane composition due to air ingress into the dissolved gas collection line.

The marked enhancement in mass transfer noted following an increase in V_L (Figs. 3 and 4) can be attributed to the maintenance of a high liquid side concentration gradient at the liquid-membrane interface at high V_L which enhances the driving force for mass transport [23]. However, for the PDMS membrane, a palpable decline in removal efficiency was simultaneously observed as V_L increased (Fig. 1). At low V_L, PDMS membrane resistance ($1/k_m$) was around 8% of the total resistance ($1/K_L$, 214,626 s m^{-1}). At high V_L, liquid phase resistance was reduced and the membrane contributed up to 99% of $1/K_L$ (19,035 s m^{-1}). The estimated membrane resistance therefore suggests that dissolved CH_4 removal is constrained by the permeability of methane through the dense PDMS polymer within the short residence time provided at high V_L. Bessarabov et al. [17] studied O_2 desorption through PDMS and observed similar behaviour (Fig. 4). However, whilst O_2 is characterised by a lower permeability coefficient ($_{Pi}$) across PDMS than methane (600 and 950×10^{-10} cm^3 (STP) cm cm^{-2} s^{-1} cm-Hg^{-1} respectively [24], the authors reported a higher mass transfer coefficient for O_2 at high V_L (Fig. 3). This observation could be attributed to the lower PDMS wall thickness used in their study (l_m, 150 μm) which also contributes to the membrane coefficient ($k_m = {}_{Pi}/l_m$) [9]. Therefore whilst a reduction in membrane wall thickness can provide some enhancement to mass transfer, mass transfer in nonporous membranes is primarily restricted by the permeability of the polymer. For comparison, the microporous membrane exhibited a resistance to mass transfer ($1/k_m$) of 102 s m^{-1} (Eq. (4)) or 0.2% of the overall mass transfer resistance ($1/K_L$ 46,729 s m^{-1}) at high V_L indicating that the membrane provides limited restriction to gas transport thus the microporous system is primarily liquid phase controlled. This was practically evidenced by continued enhancement of the mass transfer coefficient without significant deleterious impact on removal efficiency at high V_L (Figs. 1 and 4).

Sherwood analysis demonstrated that higher mass transfer can be achieved using UASB effluent in the nonporous HFMC than is predicted using analogues (Fig. 9). It is posited the enhancement identified arises from the methane supersaturation observed in the UASB effluent which increased the concentration gradient and hence the net driving force for mass transfer. This is analogous to observations made by Heile et al. [9] who identified that flux across a nonporous HFMC increased proportionately with an increase in feed side concentration. It has been suggested that it is the formation of microbubbles which induces supersaturation since the microbubbles can become entrained within the organic matrix [5]; such observation could explain why supersaturation was not determined in the AnMBR permeate which was free of organic particles. Whilst the exact mechanism behind supersaturation is as yet unclear, Hartley and Lant [5] similarly posited that CH_4 supersaturation provided the mass transfer driving force underpinning what they described as a forced stripping effect in an anaerobic system. To avoid clogging of the lumen by organic particles, the UASB effluent was processed on the shellside of the nonporous HFMC since the effluent comprised a reasonably high solids concentration (Table 2). The generalised *Sh* correlation proposed by Wickramasinghe et al. [20] to describe shell-side flow in several laboratory scale HFMC provided a reasonable approximation to the data (Fig. 6). The Reynolds exponent is about half that of commercial modules which the authors suggested was due to uneven fibre spacing limiting dispersion. It is therefore asserted in this study, that the low *Re* exponent was due to the wide interstitial spacing employed to limit clogging by the coarse aggregates in the anaerobic effluent; an effect which was successfully observed (through the Perspex shell) when processing anaerobic effluent.

4.2. Implications for process application

The wider interstitial spacing required to process UASB anaerobic effluent comprising suspended solids also limits the achievable packing density (346 m^2 m^{-3} and 4600 m^2 m^{-3} for the nonporous and micro-porous membranes respectively), yielding much lower volumetric mass transfer coefficients compared to micro-porous systems, and necessitating considerably larger volumetric sizes (Fig. 10). To intensify the process, pretreatment technology for the separation of coarse particles such as microscreens could be considered for implementation (i.e. downstream of the UASB and upstream of the HFMC), thus providing protection against the ingress of particles which would permit smaller interstitial spacing to be adopted to enhance packing density, similar to that employed in the microporous HFMC for treatment of

Table 2
Anaerobic effluent characterisation for the two anaerobic systems studied.

Parameters		UASB	Anaerobic MBR
Temperature	(°C)	18.0	14.2
Suspended solids	(mg l^{-1})	36	N/d
Particle size			
d_{10}	(μm)	9	N/d
d_{50}	(μm)	173	N/d
d_{90}	(μm)	705	N/d
Total COD	(mg l^{-1})	124	18
Soluble COD	(mg l^{-1})	45	18
Protein	(mg l^{-1})	16	N/m
Polysaccharide	(mg l^{-1})	13	N/m
BOD_5	(mg l^{-1})	61	8

N/d – None detected. N/m – None measured.

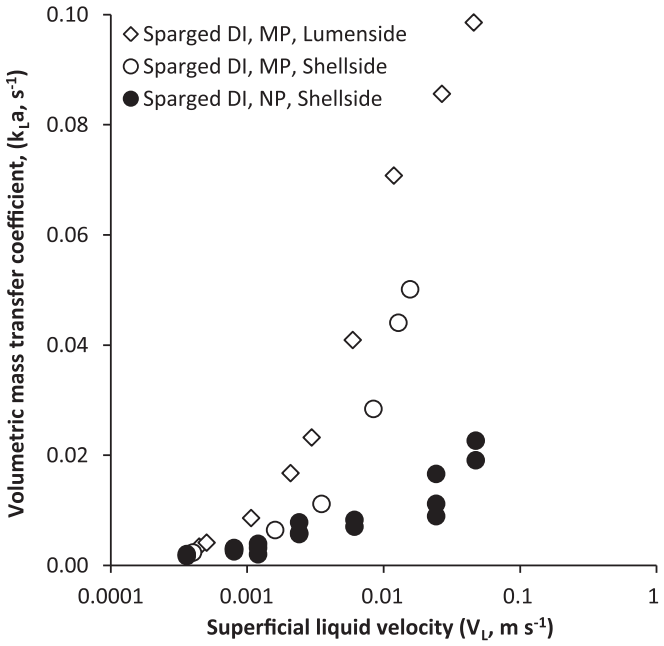

Fig. 10. Comparison of the determined volumetric mass transfer coefficients (K_La) for the non-porous and microporous membranes respectively. Data for the microporous membrane operated in both shell-side and lumen-side is presented.

AnMBR permeate. Interestingly, during trials with the micro-porous HFMC, *Sh* data produced from synthetic effluent and AnMBR permeate compared well (Fig. 7) which indicates that the low organic solute concentration in AnMBR permeate is insufficient to promote wetting in micro-porous membrane materials and further that with appropriate pretreatment, the impact of fouling or clogging on process performance is ostensibly negligible. To enhance process viability of nonporous HFMC for UASB effluent without alteration to the packing density (or to effluent pretreatment), thin film composite materials could also be considered that comprise of high permeability polymers such as poly[1-(trimethylsilyl)-1-propyne] (PTMSP) which promote considerably higher methane permeabilities ($15{,}400\times10^{-10}$ cm^3 (STP) cm cm^{-2} s^{-1} cm-Hg^{-1} [25] than PDMS markedly limiting membrane resistance for nonporous HFMC and thus enabling a reduction in process scale.

An approximation of process cost and carbon footprint was undertaken using the approach of Reed et al. [6] to establish whether: (i) carbon neutrality can be achieved through recovering a sufficient amount of dissolved methane to offset the global warming effect of any residual methane (Fig. 11); (ii) to evaluate the module configuration required to achieve a 0.14 mg l^{-1} dissolved methane consent for direct discharge to a closed conduit [2,7] (Fig. 12); and (iii) to assess whether dissolved methane recovery could be cost effective (Fig. 13). The number of modules required in series was undertaken using [26]:

$$\frac{C}{C_0} = e^{-kaL/v} \tag{9}$$

The cost index of Wickramasinghe et al. [27] was modified to include revenue from recovered methane which yields a total annualised cost (€ annum^{-1}) where a positive cost is indicative of profit. Analysis was conducted for fixed conditions of 15 °C fluid temperature, 70% methane mole fraction in the biogas phase which generates a typical saturation dissolved methane concentration of around 20 gCH$_4$ m^{-3} at equilibrium. Assessment of a single HFMC module evidences that provided dissolved methane recovery is above around 90%, the renewable electricity that can

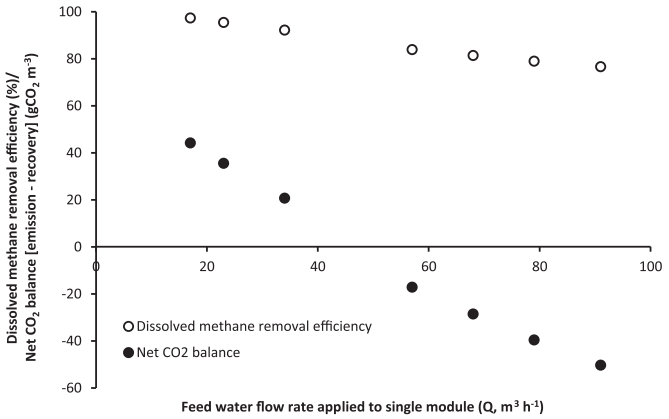

Fig. 11. Modelled dissolved methane removal efficiency estimated for a module with fibre length 0.546 m and membrane area 220 m^2. Assumed feed water saturation concentration of 20 gCH$_4$ m^{-3} (approximate equilibrium concentration to 15 °C, y_{CH_4} 70%). Net CO_2 balance is the difference between non-recovered dissolved CH_4 at the HFMC outlet (20 gCO$_2$ gCH$_4^{-1}$) and the use of the recovered fraction to offset grid electricity (0.47 kg kWh^{-1}).

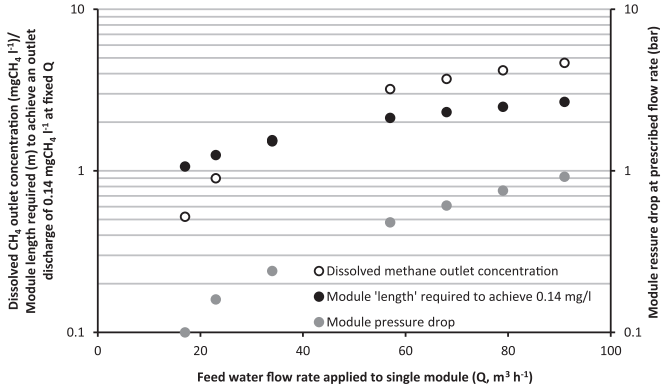

Fig. 12. Modelled dissolved CH_4 outlet concentration for fixed flow rates in a single module, the theoretical contactor length required to achieve 0.14 mgCH$_4$ l^{-1} at the HFMC outlet and indicative pressure drop data used within the modelled membrane contactor [28].

be produced from the recovered methane can offset the carbon footprint of the dissolved methane residual left in the effluent (Fig. 11). On this basis, a single module in series can be considered sufficient for treatment provided discharge is into an open water course. However, if discharge is to a closed conduit, several modules in series are required to achieve the discharge consent of 0.14 mg l^{-1} ($n=L/L_{module}$) (Fig. 12). Wickramasinghe et al. [20] identified that the optimum commercial design is weighted on most mass transferred per unit cost. This is illustrated in the U-shaped curve developed for single modules in parallel in which the left hand side is driven by membrane cost since for lower single module flows more modules are required in parallel to match total flow, whereas the right hand side of the curve is dominated by pressure drop due to the higher flow rates (i.e. velocities) used in fewer membrane modules. Importantly, the positive annualised cost is indicative that dissolved methane recovery using HFMC can be economically practicable. In practice, the economic return for discharge to a closed conduit (to achieve 0.14 mg l^{-1}) is considerably lower than for operating a single module within carbon neutral constraints. However, the economics for discharge to a closed conduit are best compared to bubble column crossflow cascades which are currently used to achieve the same discharge standard. Cascades employ long retention times (30–45 min) and high *G*/*L* ratios (10:1 to 15:1) which obviate the opportunity for recovery [8]. Consequently, microporous membranes which combine short retention times (1.5–

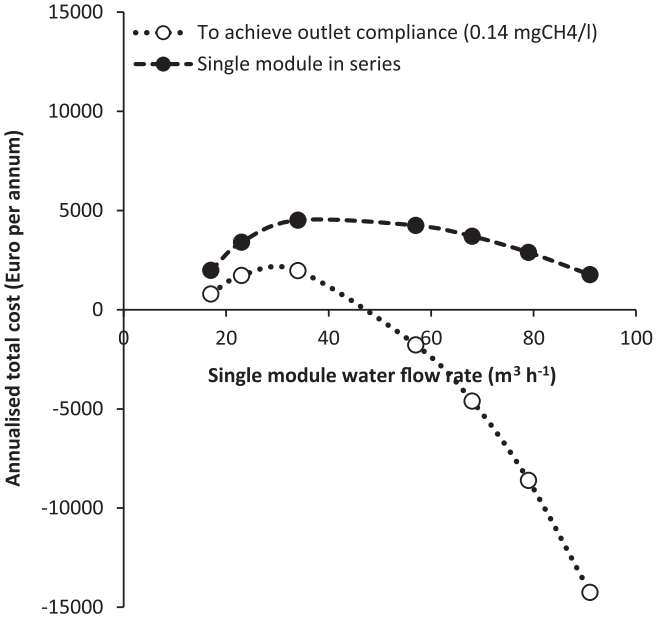

Fig. 13. Cost indices presented for dissolved methane recovery based on those of based on [27] with inclusion of a revenue component to account for methane utilisation (€0.094 kWh^{-1}; 40% electrical conversion efficiency). Cost based on a water flow of around 10,000 PE. Total number of modules in series required (total length/module length) was determined by rounding. Membrane cost used € 40 m^{-2}; 7 year life expectancy. Values above zero indicate a positive financial return.

12.5 s) and low G/L ratios, are an opportunity to achieve cost and carbon neutral methane removal at a fraction of the process footprint.

5. Conclusions

Hollow fibre membrane contactor (HFMC) systems have been successfully demonstrated for dissolved methane recovery from anaerobic effluents. Mass transfer data obtained from HFMC systems using anaerobic effluents compared favourably to that produced from analogue effluent which suggests that the effluent matrix is not limiting. Interestingly, supersaturation of the UASB anaerobic effluent increased mass transfer over that predicted from the analogue which should be considered at the design stage.

For the micro-porous HFMC, mass transfer was observed to be liquid phase controlled which implies that the membrane does not restrict mass transfer. Consequently, the AnMBR coupled microporous HFMC can be regarded the most economically favourable system, for which the financial viability was illustrated through economic modelling. However, for the nonporous HFMC, the membrane provides the principle resistance to mass transfer and as such will negatively influence process scale and economic viability for application to UASB-nonporous HFMC systems where the primary objective is to achieve either carbon neutrality or the closed conduit discharge consent (0.14 mg l^{-1}). This is further compounded by the requirement for substantial interstitial spacing included in the nonporous HFMC to limit clogging. The impact of both constraints was evidenced through the volumetric mass transfer coefficient which was markedly below that observed for the microporous HFMC. To enhance the economic viability and constrain scale of a UASB-nonporous HFMC coupled system, two options are therefore proposed: (i) enhance mass transfer through membrane material selection (reduced wall thicknesses, or use of high permeability substrates); or (ii) inclusion of coarse filtration upstream of the HFMC and downstream of the UASB to limit solids loading/clogging of the HFMC and achieve higher hollow-fibre packing densities that would enable more membrane material into a single contactor.

The independence of mass transfer on the gas phase was also demonstrated. Commercially available dissolved O_2 HFMC systems are presently able to achieve 90% dissolved O_2 removal at G/L ratios 50% below the $G/L_{minimum}$ through combined vacuum and sweep gas which substantiates the assertion that dissolved methane can be recovered in useful form without deleteriously impacting on mass transfer. Based on this assumption, revenue is illustrated to exceed cost based on recovery and reuse of methane. This is equivalent to an electricity production of around 0.12 $kWh_e\ m^{-3}$ of wastewater treated (assuming 40% conversion efficiency), which when combined with energy produced from the upstream anaerobic reactor, offers the potential to approach energy neutral wastewater treatment [6].

Acknowledgements

We thank Yorkshire Water, Severn Trent Water, Anglian Water, Northumbrian Water and the Engineering and Physical Sciences Research Council (EPSRC, V/N 08001923) for their financial support.

Nomenclature

a	Surface area per membrane volume (m^{-1})
C^*	Equilibrium concentration of dissolved methane in water (mg l^{-1})
C_e	Measure dissolved methane concentration in water (mg l^{-1})
d_e	Equivalent diameter (m)
D_g	Effective diffusion coefficient through a gas filled pore ($m^2\ s^{-1}$)
Gz	Graetz number ($[d_e/L]ReSc$) (dimensionless)
H	Dimensionless Henry's constant (28.41 for methane at 25 °C) (dimensionless)
K_L	Overall mass transfer coefficient (m s^{-1})
k_g	Individual gas mass transfer coefficient (m s^{-1})
k_l	Individual liquid mass transfer coefficient (m s^{-1})
k_m	Individual membrane mass transfer coefficient (m s^{-1})
l_m	Membrane thickness (m)
L	Membrane length in the direction of flow (m)
P	Permeability of the polymer (cm^3 cm cm^{-2} s^{-1} cm-Hg^{-1})
Q_G	Sweep gas flow rate ($m^3\ s^{-1}$)
Q_L	Feed water flow rate ($m^3\ s^{-1}$)
Re	Reynold's number ($Re=\rho d_e V_L/\mu$) (dimensionless)
Sc	Schmidt number ($Sc=\mu/\rho D_L$) (dimensionless)
Sh	Sherwood number ($Sh=kd_e/D_L$) (dimensionless)
V_G	Gas velocity within the membrane contactor (m s^{-1})
V_L	Liquid velocity within the membrane contactor (m s^{-1})
Vol_G	Gas phase volume of sample (l)
Vol_L	Liquid phase volume of sample (l)
X_{L1}	Dissolved methane concentration in sample (mg l^{-1})
X_{G1}	Headspace methane concentration in sample pre-equilibrium (mg l^{-1})
X_{G2}	Headspace methane concentration in sample post-

	equilibrium ($mg\,l^{-1}$)
y_{CH_4}	Methane mole fraction in the gas phase above the feed water (dimensionless)

Greek Letters

Θ	Packing fraction (dimensionless)
α	Bunsen solubility coefficient ($mlCH_4\,mlH_2O^{-1}$)
ε_m	Membrane porosity (dimensionless)
τ_m	Membrane tortuosity (dimensionless)

References

[1] J. Lester, B. Jefferson, A.L. Eusebi, E. McAdam, E. Cartmell, Anaerobic treatment of fortified municipal wastewater in temperate climates, J. Chem. Technol. Biotechnol. 88 (2013) 1280–1288.

[2] H.D. Robinson, M. Carville, Waste 2010: The use of pilot-scale trials in the design of state of the art leachate treatment plants, in: Proceedings of Waste 2010 Conference, 28–29 Sept., Stratford-Upon-Avon, UK, 2010.

[3] J. Cookney, E. Cartmell, B. Jefferson, E.J. McAdam, Recovery of methane from anaerobic process effluent using poly-di-methyl-siloxane membrane contactors, Water Sci. Technol. 65 (2012) 604–610.

[4] A. Pauss, G. Andre, M. Perrier, S.R. Guiot, Liquid-to-gas mass transfer in anaerobic processes: inevitable transfer limitations of methane and hydrogen in the biomethanation process, Appl. Environ. Microbiol. 56 (1990) 1636–1644.

[5] K. Hartley, P. Lant, Eliminating non-renewable CO2 emissions from sewage treatment: an anaerobic migrating bed reactor pilot plant study, Biotechnol. Bioeng. 95 (2006) 384–398.

[6] E.J. McAdam, D. Luffler, N. Martin-Garcia, A.L. Eusebi, J.N. Lester, B. Jefferson, E. Cartmell, Integrating anaerobic processes into wastewater treatment, Water Sci. Technol. 63 (2011) 1459–1466.

[7] A.M. Buswell, T.E. Larson, Methane in groundwaters, J. Am. Water Work. Assoc. 29 (1937) 1978–1982.

[8] N. Brown, Methane Dissolved in Wastewater Exiting UASB Reactors: Concentration Measurement and Methods for Neutralisation (MSc Thesis), Royal Institute of Technology, Stockholm, Sweden, 2006.

[9] S. Heile, S. Rosenberger, A. Parker, B. Jefferson, E.J. McAdam, Establishing the suitability of symmetric ultrathin wall polydimethylsiloxane hollow-fibre membrane contactors for enhanced CO_2 separation during biogas upgrading, J. Membr. Sci. 452 (2014) 37–45.

[10] J.H. O'Haver, R. Walk, B. Kitiyanan, J.H. Harwell, D.A. Sabatini, Packed column and hollow-fibre air stripping of a contaminant-surfactant stream, J. Environ. Eng. 130 (2004) 4–11.

[11] A. Sengupta, P.A. Peterson, B.D. Miller, J. Schneider, C.W. Fulk Jr, Large-scale application of membrane contactors for gas transfer from or to ultrapure water, Sep. Purif. Technol. 14 (1998) 189–200.

[12] F. Bougie, M.C. Illiuta, Analysis of Laplace-Young equation parameters and their influence on efficient CO_2 capture in membrane contactors, Sep. Purif. Technol. 118 (2013) 806–815.

[13] S. Goh, J. Zhang, Y. Lui, A.G. Fane, Fouling and wetting in membrane distillation (MD) and MD-bioreactor (MDBR) for wastewater reclamation, J. Membr. Sci. 323 (2013) 39–47.

[14] W.M.K.R.T.W. Bandara, H. Satoh, M. Sasakawa, Y. Nakahara, M. Takahashi, S. Okabe, Removal of residual methane gas in an upflow anaerobic sludge blanket reactor treating low-strength wastewater at low temperature with degassing membrane, Water Res. 45 (2011) 3533–3540.

[15] I. Martin-Garcia, V. Monsalvo, M. Pidou, P. Le-Clech, S.J. Judd, E.J. McAdam, B. Jefferson, Impact of membrane configuration on fouling in anaerobic membrane bioreactors, J. Membr. Sci. 382 (2011) 41–49.

[17] D.G. Bessarabov, E.P. Jacobs, R.D. Sanderson, I.N. Beckman, Use of nonporous polymeric flat-sheet gas-separation membranes in a membrane-liquid contactor: experimental studies, J. Membr. Sci. 113 (1996) 275–284.

[18] M. Mavroudi, S.P. Kaldis, G.P. Sakellaropoulos, A study of mass transfer resistance in membrane gas–liquid contacting processes, J. Membr. Sci. 272 (2006) 103–115.

[18] M.C.R. Alberto, J.R.M. Arah, H.U. Neue, R. Wassmann, R.S. Lantin, J.B. Aduna, K. F. Bronson, A sampling technique for the determination of dissolved methane in soil solution, Chemosphere 2 (2000) 57–63.

[19] Membrana, Minimodule membrane contactors, Membrana: A Polypore Company D86, 2012, pp. 1–2.

[20] S.R. Wickramasinghe, M.J. Semmens, E.L. Cussler, Hollow fiber modules made with hollow fiber fabric, J. Membr. Sci. 84 (1993) 1–14.

[21] X. Tan, G. Capar, K. Li, Analysis of dissolved oxygen removal in hollow fibre membrane modules: effect of water vapour, J. Membr. Sci. 251 (2005) 111–119.

[22] R. Marshall, D. Browell, S. Smith, Guidance on Gas Treatment Technologies for Landfill Gas Engines, Environment Agency LFTGN06, 2010, pp. 1–80.

[23] A. Mcleod, B. Jefferson, E.J. McAdam, Biogas upgrading by chemical absorption using ammonia rich absorbents derived from wastewater, Water Res. 67 (2014) 175–186.

[24] W.L. Robb, Thin silicone membranes – their permeation properties and some applications, Ann. NY Acad. Sci. 146 (1968) 119–137.

[25] I. Pinnau, L.G. Toy, Transport of organic vapors through poly(1-thimethylsilyl-1-propyne), J. Membr. Sci. 116 (1996) 199–209.

[26] B.W. Reed, M.J. Semmens, E.L. Cussler, Chapter 10 Membrane Contactors, in: Membrane Science and Technology, vol. 2, 1995, pp. 467–498.

[27] S.R. Wickramasinghe, M.J. Semmens, E.L. Cussler, Better hollow fibre contactors, J. Membr. Sci. 62 (1991) 371–388.

[28] Membrana, Extraflow product datasheet, Membrana: A Polypore Company D85, 2015, pp. 1–2.

[29] J.C. Crittenden, R.R. Trussell, D.W. Hand, K.J. Howe, G. Tchobanoglous, Water Treatment: Principles and Design, Wiley & Sons, New Jersey, US, 2012.

[30] S. Yamamoto, J.B. Alcauskas, T.E. Crozier, Solubility of methane in distilled water and seawater, J. Chem. Eng. Data 21 (1976) 78–80.